CHINESE JOURNAL OF PHYSICS VOL. 52, NO. 1-II February 2014

Review

Numerical Simulations of Attosecond Streaking Time Delays in Photoionization

Jing Su, Hongcheng Ni, Andreas Becker, and Agnieszka Jaroń-Becker

JILA and Department of Physics, University of Colorado, Boulder, CO 80309-0440, USA
(Received August 31, 2013)

We present results of numerical simulations and theoretical classical analysis of time delays with respect to the instant of ionization in a numerical streaking experiment. These results confirm our previous interpretation of the streaking time delay as a finite-range and field-weighted time delay. We show that in the streaking experiments the time delay strongly depends on the parameters of the streaking field. Consequently, the streaking time delay is accumulated over a finite range in space, which the emitted electron probes after its transition into the continuum until the streaking pulse ceases. Moreover, we confirm by results of our numerical simulations that the streaking time delay can be understood as a sum (or integral) over field-free time delays weighted by the relative instantaneous field strength during the propagation of the photoelectron.

DOI: 10.6122/CJP.52.404 PACS numbers: 33.80.Rv, 33.80.Wz

I. INTRODUCTION

Recently, applications of attosecond (1 as = 10^{-18} s) pulse technology led to the analysis of the question whether or not an electron is emitted instantaneously from an atom, molecule or solid upon the absorption of an extreme ultraviolet (XUV) laser photon [1–3]. One approach to observe this ultrafast dynamics of the photoelectron is the so-called attosecond streak camera technique [4]. In this approach due to the interaction with a second weak streaking pulse at a near-infrared wavelength, which is superimposed to the ionizing XUV laser pulse, the momentum of the photoelectron is modulated. Neglecting the long-range Coulomb interaction between the photoelectron and the residual target ion the momentum of the photoelectron is given by

$$\mathbf{k}_f^{(0)}(t_i) = \mathbf{k}_0 - \mathbf{A}_s(t_i), \tag{1}$$

where $k_0 = \sqrt{2(\omega - I_p)}$ is the asymptotic momentum without application of the streaking pulse and $\mathbf{A}_s(t_i)$ is the vector potential of the streaking field at the instant of transition of the photoelectron into the continuum t_i, which we denote here also as the time of ionization.

In the reported experimental data [1, 2], an oscillation of the photoelectron momentum as a function of the delay between the XUV and the near-infrared laser pulses has been observed, as expected from Eq. (1). However, the observations also revealed temporal offsets Δt_s in the oscillations as compared to the vector potential $\mathbf{A}(t_i)$, i.e.,

$$\mathbf{k}_f(t_i) \simeq \mathbf{k}_0 - \alpha \mathbf{A}_s(t_i + \Delta t_s), \tag{2}$$

where α is a fitting parameter. These temporal offsets were first interpreted as delays in the emission of the photoelectron. However, theoretical works, e.g., [5–19], showed that on the attosecond time scale of these observations a detailed analysis of the effect of the Coulomb potential on the photoelectron as well as the coupling between the Coulomb potential and the streaking field needs to be taken into account. It was expected that the observed temporal offsets are, at least partially, related to the well-known Wigner-Smith (WS) time delay [20, 21]. The latter denotes the time delay of an electron propagating in a potential towards infinity as compared to a freely propagating electron. A concern with this interpretation is related to the fact that the WS time delay does diverge for a long-range interaction, such as the Coulomb potential [21–23]. Theoretical work therefore focused on the role of short- vs. long-range part of the Coulomb potential itself as well as during the coupling between the Coulomb potential and the streaking field (e.g., [9–13]).

Recently, we reported [24] results of numerical simulations and a classical analysis, which revealed the following aspects in the interpretation of the observed temporal offsets: First, we found that the temporal offsets are related to the propagation of the photoelectron over a *finite range* in time and space instead of its propagation towards infinity, as assumed in the WS time delay. Thus, according to our interpretation any previously expressed concerns regarding the divergence of the temporal offsets are unnecessary. Furthermore, we proposed that — based on an approximate formula derived in a classical analysis — the temporal offsets can be interpreted as a sum of piecewise field-free time delays weighted by the instantaneous streaking field strength relative to the field strength at the transition of the photoelectron into the continuum.

The intention of this invited paper is to review the above aspects of the temporal offsets and support our interpretation by further results of numerical calculations. To this end, we first outline the model used in the present simulations of a streaking experiment as well as the numerical techniques applied to solve the time-dependent Schrödinger equation (TDSE). Using a short-range Yukawa potential centered at a distance of the location of photoemission, we demonstrate in different scenarios that it is the time interval between the photoemission and the end of the streaking pulse that is relevant for the observed temporal offset. Finally, we discuss the interpretation of the temporal offsets as field-weighted time delays, accumulated piecewise during the propagation of the photoelectron until the streaking pulse ceases. We end with a brief summary of our results.

II. NUMERICAL SIMULATIONS

As mentioned in the introduction, our results in a previous report [24] indicate that the temporal offsets in numerical simulations of streaking experiments are related to the propagation of the photoelectron over a finite range in time and space after its transition into the continuum upon interaction with the XUV laser pulse. To substantiate this interpretation, we consider a model system in which we add a short-range potential at a distance to the center of a Coulomb potential. Since the photoelectron is initially located in the ground state of the Coulomb potential, we can test by variation of the location of

the short-range potential and/or by variation of the parameters of the streaking pulse how this additional potential does influence the temporal offset Δt_s in the numerically obtained streaking patterns. In order to vary the location of the additional short-range potential over a large region in space, we needed to use a large space-time grid in each of our numerical simulations. In view of the numerical effort to obtain precise results on the attosecond time scale as well as the number of simulations performed we restricted our analysis to a 1D model, which is well justified by noting that for a linearly polarized laser pulse the final momentum of the photoelectron is streaked along the polarization direction [c.f., Eq. (1)].

Previously, we considered Gaussian potentials of various strength as additional short-range potentials [24]. In order to show that our conclusions are independent of the form of the model potential, we used in the present set of numerical simulations the following 1D potential (Hartree atomic units, $e = m = \hbar = 1$ are used):

$$V_{\mathrm{CY}}(x) = -\frac{Z_1}{\sqrt{x^2 + a_1}} - \frac{Z_2 e^{-\sqrt{(|x|-x_0)^2+a_3}/b}}{\sqrt{(|x| - x_0)^2 + a_2}}. \tag{3}$$

The potential $V_{\mathrm{CY}}(x)$ consists of a Coulomb potential with an effective charge $Z_1 = 4.0$ and a soft-core parameter $a_1 = 3.0$, and an additional Yukawa potential with $Z_2 = 3.0$, $a_2 = 2.0$, $a_3 = 1\times10^{-5}$, and $b = 5.0$ centered at a distance x_0 from the center of the Coulomb potential at $x = 0$. The strength of the Yukawa potential is chosen to be comparable to that of the Coulomb potential to avoid any concerns regarding the influence of this additional potential on the observed temporal offsets. As we will show below [see e.g., Fig. 1(b)] the effect of the present Yukawa potential is indeed substantial enough to draw conclusions. We have chosen the electron to be initially located in the ground state of the Coulomb potential, which has an energy of -1.9448. We have tested that this initial state is not affected by the additional Yukawa potential as long as the center of the Yukawa potential is located at distances of $x_0 \geqslant 50$.

In our streaking simulations we have numerically solved the corresponding TDSE

$$i\frac{\partial\Psi(x,t)}{\partial t} = \left[\frac{p^2}{2} + V_{\mathrm{CY}}(x) + (E_{\mathrm{XUV}}(t) + E_s(t))\, x\right]\Psi(x,t), \tag{4}$$

with the momentum operator p. The electric fields of both the XUV, $E_{\mathrm{XUV}}(t)$, and the streaking laser pulse, $E_s(t)$, are represented as

$$E(t) = E_0 \sin^2(\pi t/T)\cos(\omega t + \phi), \tag{5}$$

where E_0 is the peak amplitude, T is the pulse duration, ω is the central frequency, and ϕ is the carrier-envelope phase (CEP) of the respective field. The TDSE was solved on a sufficiently large grid in space and time using the Crank-Nicolson method. We confirmed that in all simulations the outgoing wave packet stays on the grid until both pulses ceased.

The momentum distributions were obtained by spatially separating the ionized wave packet from the total wave function, which is possible due to the long propagation times used in our simulations, and then performing a Fourier transform. By varying the delay t_i

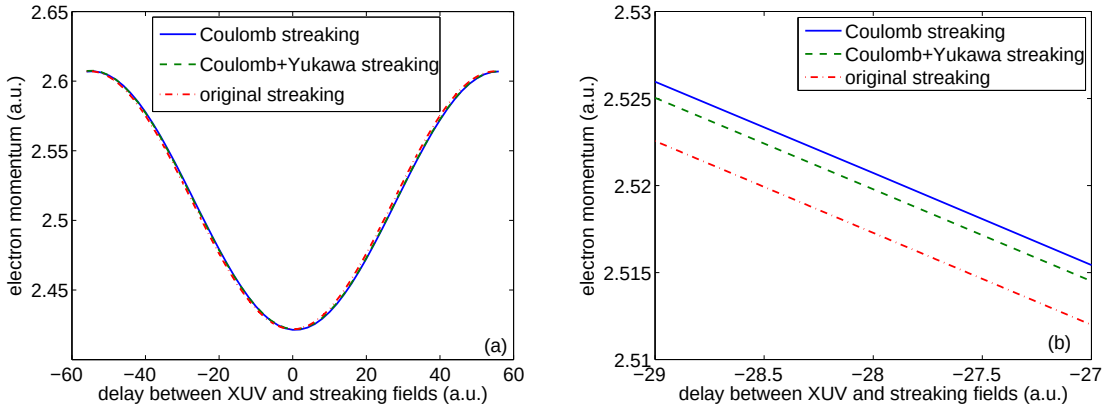

FIG. 1: (Color online) Final electron momentum as a function of the delay between XUV and streaking pulses (only the central cycle of the streaking pulse is shown). Streaking traces from numerical simulations with the Coulomb potential (blue solid line) and the combined Coulomb and Yukawa potential with $x_0 = 700$ (green dashed line) are compared. As a reference, the trace expected from the original streaking formula, Eq. (1), (red dash-dotted line) is also shown. Panel (b) is a magnification of the streaking traces to show the attosecond delay or temporal offset between them. Laser parameters are: $I_{\rm XUV} = 1 \times 10^{15}$ W/cm^2, $\omega_{\rm XUV} = 140$ eV, $T_{\rm XUV} = 600$ as, $\phi_{\rm XUV} = -\pi/2$, $I_s = 1 \times 10^{12}$ W/cm^2, $\lambda_s = 800$ nm, $N_s = 8$ cycle, and $\phi_s = -\pi/2$.

between the XUV and the streaking pulses we obtained the streaking trace as the expectation value of the final momentum of the photoelectron k_f as a function of t_i (e.g., see Fig. 1). As expected, the distributions have a temporal offset or delay Δt_s with respect to the vector potential (red dotted line) at t_i. The comparison of the streaking traces obtained in simulations with (green dashed line) and without (blue solid line) the additional Yukawa potential shows that the Yukawa potential has a substantial effect on the temporal offset. We then extracted Δt_s by fitting the momentum trace to the expression in Eq. (2) using the least-square method for the fitting parameters α and Δt_s.

III. INTERPRETATION OF STREAKING TIME DELAYS

In order to interpret the results of our numerical simulations, presented below, we also performed a classical analysis of the streaking process. To this end, we model the propagation of an electron in the continuum by Newton's equation [25]:

$$\frac{dk}{dt} = -E_s(t) - \frac{dV}{dx}. \tag{6}$$

By multiplying dx to both sides and then integrating, the solution for the asymptotic momentum of the electron at $x \to \infty$ is given by [24]

$$k_f(t_i) = \sqrt{k_0^2 - 2\int_{t_i}^{T} E_s(t)k(t)dt}, \tag{7}$$

with $k_0 = \sqrt{2(\omega - I_p)}$ and t_i as the time delay of photoelectron emission. We note that in Eq. (7) the integral over time is effectively limited by the end of the streaking pulse since $E_s(t)$ appears as a factor in the integrand. We then equal this result to the streaking formula, Eq. (2),

$$\begin{aligned} k_f(t_i) &\simeq k_0 - \alpha A_s(t_i + \Delta t_s) \\ &\simeq k_0 - \alpha A_s(t_i) + \alpha E_s(t_i)\Delta t_s \end{aligned} \tag{8}$$

to get [for $E_s(t_i) \neq 0$]

$$\Delta t_s \simeq \frac{\alpha A_s(t_i) + \sqrt{k_0^2 - 2\int_{t_i}^{T} E_s(t)k(t)dt} - k_0}{\alpha E_s(t_i)}. \tag{9}$$

We note that in the above approximation the time delay depends on the choice of the initial position x_i and the parameter α. We have chosen x_i to be the expectation value of the electron position in the initial state, i.e., $x_i = 0$ for $V_{\mathrm{CY}}(x)$. Furthermore, we determined α such that Δt_s remains approximately constant while varying t_i typically over the central cycle of the streaking pulse (see Fig. 2 in Ref. [24]).

III-1. Finite-rage time delays

As mentioned above, the integral in Eq. (7) is limited by the instants of transition of the photoelectron into the continuum, t_i, and the end of the streaking pulse, T. Thus, according to our classical analysis the observed time delay is accumulated during the propagation of the photoelectron over this finite time interval. For this reason, the range of the potential that has to be taken into account is well determined and limited, since the photoelectron propagates over a finite distance in space from t_i to T. This is in contrast to the WS time delay, which accounts for the full range of the potential, i.e., for a long-range Coulomb potential in 1D up to $x \to \infty$. Thus, due to the finite limits in our classical analysis the temporal offset Δt_s does not diverge (for a streaking pulse with finite pulse duration), in agreement with the observations in the experiment and in contrast to the assumption that a (diverging) WS time delay is part of the observed temporal offset.

To test this conclusion from our classical analysis we performed a series of numerical simulations using the model potential, Eq. (3), by varying the position of the Yukawa potential with respect to the center of the Coulomb potential. In the first set of calculations we have chosen a 6-cycle streaking pulse at 800 nm with a peak intensity of $I_s = 1 \times 10^{12}$ W/cm^2, and a CEP of $\phi_s = -\pi/2$. To photoionize the electron, we used an XUV pulse with $I_{\mathrm{XUV}} = 1 \times 10^{15}$ W/cm^2, $\omega_{\mathrm{XUV}} = 100$ eV, $\tau_{\mathrm{XUV}} = 600$ as, and $\phi_{\mathrm{XUV}} = -\pi/2$. Quantum

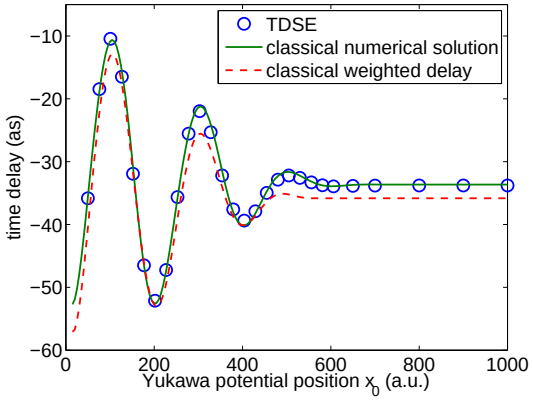

FIG. 2: (Color online) Streaking time delay as a function of the position of the Yukawa potential. The TDSE results (blue open circles) are compared with the predictions based on the classical Eqs. (9) (green solid line) and (15) (red dashed line). Laser parameters are given in the text.

results in Fig. 2 (blue open circles) confirm our expectation that only a finite range of the combined Coulomb-Yukawa potential takes effect in a streaking experiment, since the streaking time delay remains constant if the Yukawa potential is located at far distances, here $x_0 \gtrsim 650$. We have checked that the constant time delay for $x_0 \gtrsim 650$ is equal to the streaking time delay obtained without the additional Yukawa potential. These results clearly show that the obtained time delays do not account for the presence of the Yukawa potential, if it is located at far distances from the location of photoemission of the electron.

Furthermore, our classical predictions from Eq. (9) for Δt_s (green solid lines) agree very well with the TDSE results (blue open circles). From Eq. (9), we see that Δt_s depends on the coupling between the streaking field and the potential and, thus, on both the parameters of the streaking field $E_s(t)$ and the shape of the potential. Thus, we expect that the streaking time delay can be indeed interpreted via the classical dynamics of the photoelectron in the combined potential of the Coulomb and streaking fields over a *finite range* in time and space until the streaking pulse ceases at $t = T$.

To further confirm these expectations we performed further sets of numerical simulations. In these simulations we varied the XUV photon energy (Fig. 3) or the shape and length of the streaking pulse (Fig. 4), respectively. We varied these two laser parameters in order to change either the momentum or the propagation time of the photoelectron until the streaking pulse ceases. With both changes we therefore control the propagation distance of the photoelectron while the streaking pulse is present. In the first of the two sets of simulations we used a 8-cycle, 800 nm streaking pulse with an intensity of $I_s = 1 \times 10^{12}$ W/cm^2, and a CEP of $\phi_s = -\pi/2$. In the second set we applied a 3-cycle, 800 nm streaking pulse with the same peak intensity and CEP and an additional pedestal. The form of the latter field envelope was given by

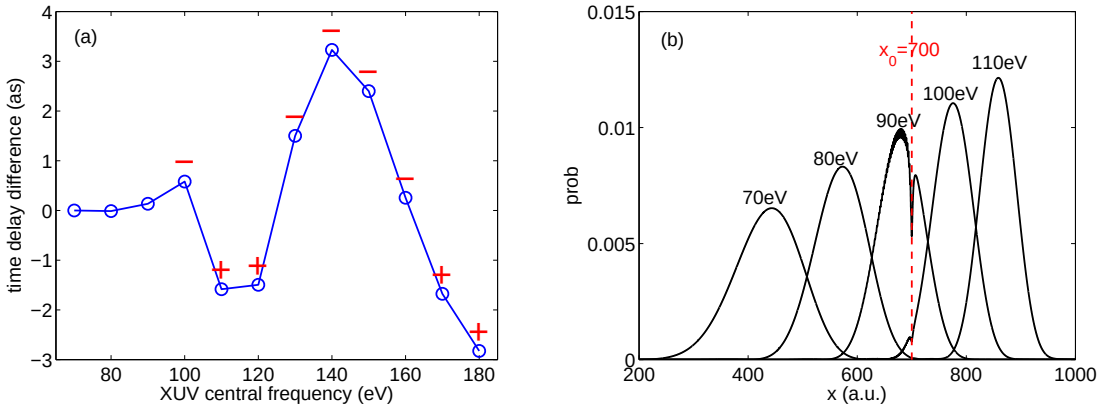

FIG. 3: (Color online) (a) Difference in the streaking time delay (blue solid line with open circles) obtained with and without Yukawa potential as a function of XUV central frequency. Assuming the electron is ionized at the peak of the streaking field, we show the signs (red plus or minus symbols) of the streaking field at the instant when the electron wave packet arrives at the Yukawa potential for each of the data points. (b) Position of the electron wave packet at the end of the streaking field for the first five XUV frequencies used in this set of simulations [see panel (a)]. The Yukawa potential was located at the distance $x_0 = 700$, which is marked by a red dashed line. The wave packet is chosen to be liberated at the center of the streaking pulse and each wave packet is normalized to 1 for the sake of comparison. Laser parameters are given in the text.

$$E_{\rm env}(\beta_p, T_p) = \begin{cases} E_0 \sin^2(\pi t/T_s) & 0 \le t \le T_s/2, \\ (1-\beta_p)E_0 \sin^2(\pi t/T_s) + \beta_p E_0 \cos^2\left[\frac{\pi(t-T_s/2)}{T_s+2T_p}\right] & T_s/2 \le t \le T_s, \\ \beta_p E_0 \cos^2\left[\frac{\pi(t-T_s/2)}{T_s+2T_p}\right] & T_s \le t \le T_s + T_p, \\ 0 & \text{else}, \end{cases} \tag{10}$$

in which $\beta_p = 0.2$ and the length of the pedestal is determined by T_p. For the XUV parameters, we have chosen $I_{\rm XUV} = 1 \times 10^{15}$ W/cm^2, $\tau_{\rm XUV} = 600$ as, $\phi_{\rm XUV} = -\pi/2$ as in all simulations, and $\omega_{\rm XUV} = 100$ eV for the latter set.

In Fig. 3 (a), we present the difference between the streaking time delays obtained with and without the Yukawa potential as a function of the XUV central frequency. To relate the streaking time delay to the propagation distance of the photoelectron during the presence of the streaking pulse, we show in panel (b) the normalized ionized wave packet at the end of streaking pulse as a function of x for the five lowest XUV photon energies considered in this set of simulations. As a reference, the position of the Yukawa potential is marked by a red dashed line. We find, as expected, that the difference between the time delays obtained with and without the additional short-range potential does equal zero, when the ionized wave packet does not reach the location of the Yukawa potential until the streaking pulse ceases, i.e., for $\omega_{\rm XUV} \le 80$ eV in the present set of simulations. For

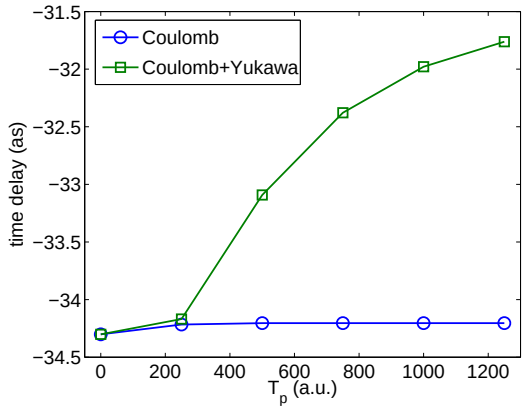

FIG. 4: (Color online) Streaking time delay as a function of the pedestal length for photoionization in two potentials: Coulomb (blue solid line with circles) and Coulomb+Yukawa with $x_0 = 700$ (green solid line with squares). Laser parameters are given in the text.

larger XUV photon energies, the two time delays deviate due to the influence of the Yukawa potential, which is then reached by the ionized wave packet.

The same conclusion can be drawn from the results in Fig. 4, in which we present the streaking time delays with and without the Yukawa potential as a function of the pedestal length [c.f., Eq. (10)]. In this set of simulations the wave packet reached the location of the Yukawa potential at $x_0 = 700$ for streaking pulses with a pedestal length of $T_p \gtrsim 200$. Clearly, the two streaking delays deviate for a longer pedestal, which again confirms our interpretation of a finite-range time delay, in which the range is determined by the propagation distance of the photoelectron until the end of the streaking pulse.

III-2. Field-weighted time delays

As mentioned at the outset, using further approximations our classical analysis provides another interesting interpretation in the form of field-free time delays. To this end, we note that the momentum shift $k_f(t_i) - k_0$ in Eq. (7) is usually small. We can therefore expand the square root to first order and by setting $\alpha = 1$ we obtain

$$\Delta t_s \simeq \frac{1}{E_s(t_i)} \int_{t_i}^{T} E_s(t) \left(1 - \frac{k(t)}{k_0}\right) dt, \tag{11}$$

or by rewriting the integral as a sum

$$\Delta t_s \simeq \frac{1}{E_s(t_i)} \sum_{j=1}^{N} E_s(t_j) \Delta t^{(j)}, \tag{12}$$

with

$$\Delta t^{(j)} = \left(1 - \frac{k(t_j)}{k_0}\right) \delta t, \tag{13}$$

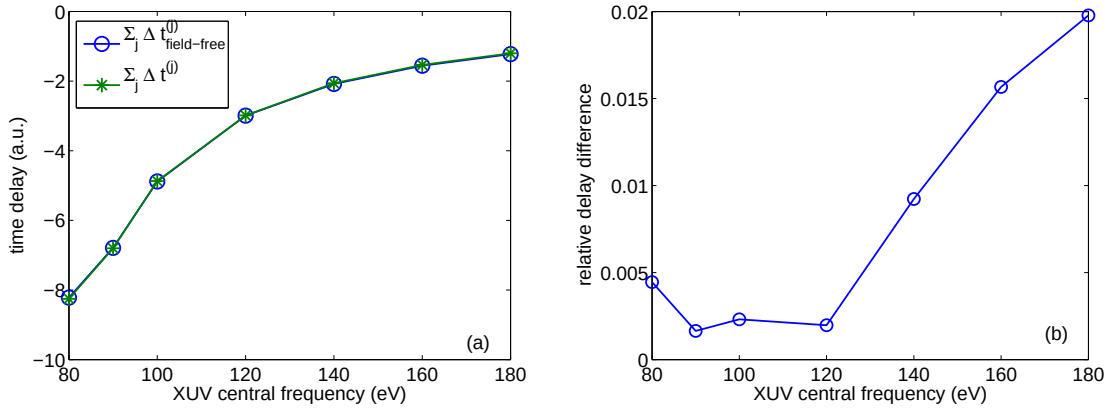

FIG. 5: (Color online) (a) Time delays $\sum_j \Delta t^{(j)}$ and $\sum_j \Delta t^{(j)}_{\text{field-free}}$ as a function of the XUV central frequency. The time delays were calculated using the back-propagation method introduced in [22, 23] for an electron propagating in the Coulomb+Yukawa potential ($\sum_j \Delta t^{(j)}_{\text{field-free}}$, blue solid line with circles) and an electron propagating in the combined potential of the streaking and Coulomb+Yukawa fields ($\sum_j \Delta t^{(j)}$, green solid line with stars). (b) Relative difference between the two time delays as a function of the XUV central frequency. All calculations were performed with the same laser parameters as in Fig. 3, while the XUV pulse was applied at the peak of the streaking field in the forward-propagation step.

where we assumed that the streaking field and the electron momentum are approximately constant in the time interval $[t_j, t_j + \delta t]$, i.e., $E_s(t) \simeq E_s(t_j)$ and $k(t) \simeq k(t_j)$ in the corresponding time interval.

We note that Eq. (13) is the classical expression for the time delay accumulated by the photoelectron in the *combined* potential of the Coulomb and the streaking fields as compared to the propagation of a free photoelectron in the corresponding region $[x_j, x_j+\delta x]$. Thus, this expression is similar to that for the (classical) WS time delay with the important difference that the expression in Eq. (13) relates to the propagation over a piecewise *finite* distance while the WS time delay accounts for the propagation to infinity.

We further note that for a weak streaking field the time delay $\Delta t^{(j)}$ can be well approximated by neglecting the influence of the streaking field on $k(t)$ as [22, 23]:

$$\Delta t^{(j)} \simeq \Delta t^{(j)}_{\text{field-free}} = \left(1 - \frac{k_{\text{field-free}}(t_j)}{k_0}\right) \delta t. \tag{14}$$

To show this we compare in Fig. 5 results for $\sum_j \Delta t^{(j)}$ and $\sum_j \Delta t^{(j)}_{\text{field-free}}$ for typical laser parameters used in the present streaking simulations. The corresponding time delays were obtained using the back-propagation method introduced in Refs. [22, 23]. It can be clearly seen from the results that the streaking field has negligible influence on this time delay.

Using this additional approximation the streaking time delay finally yields:

$$\Delta t_s \simeq \sum_{j=1}^{N} \frac{E_s(t_j)}{E_s(t_i)} \Delta t^{(j)}_{\text{field-free}}. \tag{15}$$

As mentioned above, $\Delta t^{(j)}_{\text{field-free}}$ is the finite-range piecewise field-free time delay that the electron accumulates during its propagation in the time interval $[t_j, t_j + \delta t]$ and over a related finite region $[x_j, x_j + \delta x]$ of the potential $V(x)$ as compared to the propagation of a free particle over the same distance in space.

Predictions based on Eq. (15) (red dashed line) are in good agreement with those of the full TDSE results as well as those based on Eq. (9), as exemplified in Fig. 2. Thus, we can give the following interpretation: The observed streaking time delay is neither the WS time delay nor the simple sum of finite-range piecewise field-free time delays. Instead, it can be understood as a field-weighted time delay, in which the piecewise field-free time delays are weighted by the streaking field strength present when the electron wave packet propagates over the corresponding part of the potential.

We finally point out that the influence of the instantaneous field strength on the observed time delay can be also seen from the results in Fig. 3(a). To this end, we note that according to our interpretation the difference between the streaking time delays with and without the additional Yukawa potential, as presented in Fig. 3(a), is approximately given by the contribution to the streaking time delay caused by the presence of the Yukawa potential as:

$$\Delta t^{\text{Y}}_s(x_0, \omega_{\text{XUV}}) \simeq \frac{E_s(t_{\text{Y}})}{E_s(t_i)} \Delta t^{\text{Y}}_{\text{WS}}, \tag{16}$$

where t_i and t_{Y} are the instant of ionization and the time instant at which the electron reaches the Yukawa potential, respectively, and $\Delta t^{\text{Y}}_{\text{WS}}$ is the WS time delay induced by the Yukawa potential. Since $E_s(t_i) > 0$ in the present simulations and one can show that $\Delta t^{\text{Y}}_{\text{WS}} < 0$, we expect that the sign of the time delay difference should be opposite to the sign of the instantaneous field strength as the photoelectron reaches the Yukawa potential. The latter were retrieved from the actual numerical simulations and are marked in Fig. 3(a) for each of the simulations. It is seen that our expectation of a difference in sign between the time delay difference and the instantaneous field strength is indeed confirmed.

IV. CONCLUSIONS

In summary, we presented numerical simulations of streaking experiments using a model system consisting of a 1D Coulomb potential and an additional short-range Yukawa potential at a distance to the center of the Coulomb potential. By varying the location of the Yukawa potential and the field parameters of the streaking pulse we were able to confirm two aspects of the streaking time delay, which we proposed in a previous report [24]. First, the streaking time delay is accumulated by the photoelectron after the transition into

the continuum over a finite range in time and space until the streaking pulse ends. Next, the streaking time delay can be understood as a sum of piecewise field-free time delays weighted by the instantaneous field strength during the propagation of the photoelectron in the potential.

Acknowledgments

J.S. and A.B. acknowledge support by a grant from the U.S. Department of Energy, Division of Chemical Sciences, Atomic, Molecular and Optical Sciences Program. H.N. was supported via a grant from the U.S. National Science Foundation (Award No. PHY-0854918). A.J.-B. was supported by grants from the U.S. National Science Foundation (Award No. PHY-1125844 and Award No. PHY-1068706). This work utilized the Janus supercomputer, which is supported by the National Science Foundation (award number CNS-0821794) and the University of Colorado Boulder. The Janus supercomputer is a joint effort of the University of Colorado Boulder, the University of Colorado Denver and the National Center for Atmospheric Research. Janus is operated by the University of Colorado Boulder.

References

[1] A. L. Cavalieri, N. Müller, T. Uphues, V. S. Yakovlev, A. Baltuška, B. Horvath, B. Schmidt, L. Blümel, R. Holzwarth, S. Hendel, M. Drescher, U. Kleineberg, P. M. Echenique, R. Kienberger, F. Krausz, and U. Heinzmann, Nature **449**, 1029 (2007).
[2] M. Schultze, M. Fieß, N. Karpowicz, J. Gagnon, M. Korbman, M. Hofstetter, S. Neppl, A. L. Cavalieri, Y. Komninos, T. Mercouris, C. A. Nicolaides, R. Pazourek, S. Nagele, J. Feist, J. Burgdörfer, A. M. Azzeer, R. Ernstorfer, R. Kienberger, U. Kleineberg, E. Goulielmakis, F. Krausz, and V. S. Yakovlev, Science **328**, 1658 (2010).
[3] K. Klünder, J. M. Dahlström, M. Gisselbrecht, T. Fordell, M. Swoboda, D. Guénot, P. Johnsson, J. Caillat, J. Mauritsson, A. Maquet, R. Taïeb, and A. L'Huillier, Phys. Rev. Lett. **106**, 143002 (2011).
[4] J. Itatani, F. Quéré, G. L. Yudin, M. Y. Ivanov, F. Krausz, and P. B. Corkum, Phys. Rev. Lett. **88**, 173903 (2002).
[5] A. S. Kheifets and I. A. Ivanov, Phys. Rev. Lett. **105**, 233002 (2010).
[6] I. A. Ivanov, Phys. Rev. A **83**, 023421 (2011).
[7] I. A. Ivanov, Phys. Rev. A **86**, 023419 (2012).
[8] C.-H. Zhang and U. Thumm, Phys. Rev. A **84**, 033401 (2011).
[9] S. Nagele, R. Pazourek, J. Feist, K, Doblhoff-Dier, C. Lemell, K. Tökési, and J. Burgdörfer, J. Phys. B **44**, 081001 (2011).
[10] M. Ivanov and O. Smirnova, Phys. Rev. Lett. **107**, 213605 (2011).
[11] J. M. Dahlström, A. L'Huillier, and A. Maquet, J. Phys. B **45**, 183001 (2012).
[12] J. M. Dahlström, D. Guénot, K. Klünder, M. Gisselbrecht, J. Mauritsson, A. L'Huillier, A. Maquet, and R. Taëb, Chem. Phys. **414**, 53 (2013).
[13] S. Nagele, R. Pazourek, J. Feist, and J. Burgdörfer, Phys. Rev. A **85**, 033401 (2012).
[14] R. Pazourek, J. Feist, S. Nagele, and J. Burgdörfer, Phys. Rev. Lett. **108**, 163001 (2012).

[15] C.-H. Zhang and U. Thumm, Phys. Rev. A **82**, 043405 (2010).
[16] J. C. Baggesen and L. B. Madsen, Phys. Rev. Lett. **104**, 043602 (2010).
[17] M. D. Spiewanowski and L. B. Madsen, Phys. Rev. A **86**, 045401 (2012).
[18] R. Pazourek, S. Nagele, and J. Burgdörfer, Faraday Discuss. **163**, 353 (2013).
[19] L. R. Moore, M. A. Lysaght, J. S. Parker, H. W. van der Hart, and K. T. Taylor, Phys. Rev. A **84**, 061404 (2011).
[20] E. P. Wigner, Phys. Rev. **98**, 145 (1955).
[21] F. T. Smith, Phys. Rev. **118**, 349 (1960).
[22] J. Su, H. Ni, A. Becker, and A. Jaroń-Becker, Phys. Rev. A **87**, 033420 (2013).
[23] J. Su, H. Ni, A. Becker, and A. Jaroń-Becker, J. Mod. Opt. **60**, 1484 (2013).
[24] J. Su, H. Ni, A. Becker, and A. Jaroń-Becker, Phys. Rev. A **88**, 023413 (2013).
[25] P. B. Corkum, Phys. Rev. Lett. **71**, 1994 (1993).